

Superresolution of Radar Forward-Looking Imaging Based on Accelerated TV-Sparse Method

Yin Zhang , Member, IEEE, Qiping Zhang , Graduate Student Member, IEEE, Yongchao Zhang , Member, IEEE, Yulin Huang , Senior Member, IEEE, and Jianyu Yang , Member, IEEE

Abstract—Total variation-sparse (TV-sparse)-based multiconstraint deconvolution method has been used to realize superresolution imaging and preserve target contour information simultaneously of radar forward-looking imaging. However, due to the existence of matrix inversion, it suffers from high computational complexity, which restricts the ability of radar real-time imaging. In this article, an Gohberg–Semencul (GS) decomposition-based fast TV-sparse (FTV-sparse) method is proposed to reduce the computational complexity of TV-sparse method. The acceleration strategy utilizes the low displacement rank features of Toeplitz matrix, realizing fast matrix inversion by using a GS representation. It reduces the computational complexity of traditional TV-sparse method from $O(N^3)$ to $O(N^2)$, benefiting for improvement of the computing efficiency. The simulation and experimental data processing results show that the proposed FTV-sparse method has almost no resolution loss compared with the traditional TV sparse method. Hardware test results show that the proposed FTV-sparse method significantly improves the computational efficiency of TV-sparse method.

Index Terms—Gohberg–Semencul (GS) representation, radar imaging, superresolution, sparse, total variation.

I. INTRODUCTION

REAL-aperture radar can obtain the target information of forward-looking area through antenna scanning, benefiting for autonomous landing, autopilot, and topographic mapping and many other applications [1]–[4]. The range resolution can be improved by transmitting linear frequency modulated signal and making pulse compression. However, due to the limitation of antenna size, the azimuth resolution is limited. In practice, the azimuth resolution needs to be improved to match range resolution.

According to Rayleigh criterion, targets with a distance smaller than the Rayleigh distance (RD) are located at the same resolution cell and cannot be distinguished separately, where RD is the space between the peak of the antenna pattern and the first zero-crossing [5]–[7]. This shows that the resolution of real

aperture imaging cannot beyond one beam width. Therefore, in order to obtain high azimuth resolution radar image, it is necessary to transmit narrow antenna beam in azimuth, which requires large antenna aperture. However, due to the limitation of the platform in practical application, the antenna cannot be infinitely enlarged usually.

Superresolution technology provides the possibility to improve the resolution breaking Rayleigh limit without changing the hardware conditions [8]–[10]. Previous researchers have proposed many superresolution methods to improve azimuth resolution in forward-looking imaging [11]. In [12], the Wiener filtering method was proposed to realize superresolution; however, the resolution improvement is limited especially in the condition of low signal-to-noise ratio (SNR). The truncated singular value decomposition (TSVD) method can suppress noise amplification by truncating the smaller singular value, but the resolution improvement is very limited [13]. Spectrum estimation based methods, such as Capon [14], [15], multiple signal classification [16], [17], and so on, can improve the resolution, but they need multiple snapshots, and their performance is poor in the case of single snapshot. Iterative adaptive approach needs only one snapshot, but suffers from high computational complexity [18], [19]. Sparse regularization method can efficiently improve the resolution, but it only considers the improvement of the resolution, not the preservation of the target contour information [20]–[22]. The total variation (TV) method can preserve the contour of the target, but it is sensitive to noise and has limited resolution improvement [23], [24].

Considering simultaneously improving resolution and preserving target contour, a TV-sparse based multiconstraint deconvolution method was proposed in our previous literature [25]. This method simultaneously introduces sparse and TV constraints in the framework of regularization, enhancing both the resolution and target contour. However, due to the need of matrix inversion, this method suffers from high computational complexity, which is the order of $O(N^3)$. In radar imaging, the dimension of echo is usually large, and the real-time performance of TV-sparse method will be greatly restricted by inversion operation. Therefore, the acceleration method needs to be studied to improve the real-time superresolution ability of TV-sparse method.

In order to solve the problem of high computation cost caused by matrix inversion, researchers typically wish to realize fast inversion by utilizing special structures of coefficient matrix to avoid the inversion operation, such as Toeplitz structure, Hankel

Manuscript received August 7, 2020; revised September 29, 2020; accepted October 22, 2020. Date of publication October 26, 2020; date of current version January 6, 2021. This work was supported in part by the National Natural Science Foundation of China under Grant 61671117, Grant 61901090, and 61901092. (Corresponding author: Qiping Zhang.)

The authors are with the School of Information and Communication Engineering, University of Electronic Science and Technology of China, Chengdu 611731, China (e-mail: yinzhang@uestc.edu.cn; qiping_zhang@126.com; zhang_yongchao1@163.com; yulinhuang@uestc.edu.cn; jyyang@uestc.edu.cn).

Digital Object Identifier 10.1109/JSTARS.2020.3033823

structure, and so on [26], [27]. In previous research, we found that the coefficient matrix, which needs to be inverted has an approximate Toeplitz structure, which provides the possibility for fast inversion. Kailath [28] proposed the concepts of displacement structure and displacement rank, as well as revealing that the operation can be compressed by using a Toeplitz matrix. It has been proven that the displacement rank of a Toeplitz matrix is very small and, so, its inverse matrix also has a displacement structure, which laid the theoretical foundation for the fast solution of Toeplitz equations [29], [30]. Recently, utilizing the low displacement rank features of Toeplitz matrices, along with the Gohberg–Semencul (GS) representation, the fast inversion of Toeplitz matrices has been studied [31].

In this article, a GS representation based fast TV-sparse (FTV-sparse) method is proposed to achieve real-time superresolution imaging and preserve the contour of targets. First, the azimuth signal of radar forward-looking imaging is analyzed, and the azimuth echo is modeled as a convolution of antenna pattern and targets distribution. Second, considering both the resolution improvement and contour preservation of targets, the sparse and TV combination constraints are introduced in the framework of regularization, converting the superresolution problem into a convex optimization problem. Third, based on the low displacement rank features of Toeplitz matrices, along with the GS representation, an accelerate strategy is utilized to realize fast inversion of matrix. After acceleration, the computation complexity is greatly reduced. Finally, the performance of the proposed method is verified by simulation and measured data processing.

The remainder of this article is organized as follows. In Section II, the imaging mechanism of radar forward-looking imaging is analyzed, and the convolution model of azimuth echo is obtained. In Section III, the proposed method is deduced in detail. In Section IV, simulation and measured data are processed to verify the performance of the proposed method. The conclusion is discussed in Section V.

II. PROBLEM FORMULATION

A. Resolution of Radar

In radar imaging, resolution refers to the ability of radar to distinguish adjacent targets. Usually the radar echo is a two-dimensional image in range and azimuth dimensions. In range dimension, the resolution can be improved by pulse compression. The resolution after pulse compression is determined by the bandwidth of the transmitted signal, which can be expressed as

$$\rho_r = \frac{c}{2B} \quad (1)$$

where ρ_r is the range resolution, c is the light speed, and B is the bandwidth of the transmitted signal. High range resolution image can be obtained by transmitting wide bandwidth signal.

In azimuth dimension, resolution mainly depends on antenna aperture, expressing as

$$\rho_a \propto R \frac{\lambda}{D} \quad (2)$$

where R is the range, λ is the wavelength of the transmitted signal, and D is the aperture size of the antenna, which refers

to the effective area of the antenna receiving target scattering. A large antenna aperture can generate a narrow beam. According to the Rayleigh criterion, the higher the resolution.

Obviously the high azimuth resolution requires large antenna aperture. However, in practical applications, the antenna aperture is often limited by platforms, such as helicopters and missiles. Usually, azimuth resolution of radar cannot be improved by increasing real antenna aperture.

For synthetic aperture radar (SAR) imaging, the cross-range signal can be modeled as a convolution of transmitted signal and target distribution [32], [33]. Since the convolution matrix contains gradient information, its resolution can be improved by matched filtering. After matched filtering, the cross-range resolution up to

$$\rho_{\text{asar}} = \frac{D}{2} \quad (3)$$

where ρ_{asar} is the cross-range resolution of SAR.

For real-aperture radar, although its azimuth resolution can also be modeled as a convolution of antenna pattern and target distribution. However, because the convolution matrix does not contain gradient information and there is a phase matrix effect, matched filtering cannot be performed. Therefore, deconvolution methods are often used for improving its azimuth resolution.

B. Signal Model of Radar Forward-Looking Imaging

Radar realizes forward-looking imaging through antenna scanning. The radar actively emits electromagnetic waves and scans the imaging area with the motion of the platform. The resolution of the received echo is usually very low, so it is difficult to distinguish the interested target in range and azimuth. For the low-resolution echo, we first compress the pulse in the range direction and correct the range walk to realize the range high-resolution imaging.

In the previous study, we have obtained that the azimuth echo after pulse compression and range walk correction can be modeled as the convolution of target scattering and antenna pattern [25], that is

$$\mathbf{s} = \mathbf{h} \otimes \mathbf{f} \quad (4)$$

where \mathbf{s} and \mathbf{f} are the azimuth echo and target distribution, respectively; \mathbf{h} is the antenna pattern and \otimes is the convolution operator. In practical application, the echo is inevitably disturbed by noise. Considering the influence of additive white Gaussian noise and the convenience of signal processing, the convolution model shown in (4) can be discretized, i.e.,

$$\tilde{\mathbf{s}} = \mathbf{A}\mathbf{f} + \mathbf{n} \quad (5)$$

where $\tilde{\mathbf{s}} = [\tilde{\mathbf{s}}_1 \ \tilde{\mathbf{s}}_2 \ \cdots \ \tilde{\mathbf{s}}_M]^T$ is the noise-polluted echo, $\tilde{\mathbf{s}}_i = [\tilde{s}_{i1} \ \tilde{s}_{i2} \ \cdots \ \tilde{s}_{iN}]$, $i \in [1, M]$, M and N denote the sampling numbers in range and azimuth, respectively,

$$\mathbf{A} = \begin{bmatrix} \mathbf{H} & \mathbf{0} & \cdots & \mathbf{0} \\ \mathbf{0} & \mathbf{H} & \ddots & \vdots \\ \vdots & \ddots & \ddots & \mathbf{0} \\ \mathbf{0} & \mathbf{0} & \cdots & \mathbf{H} \end{bmatrix}_{MN \times MN}$$

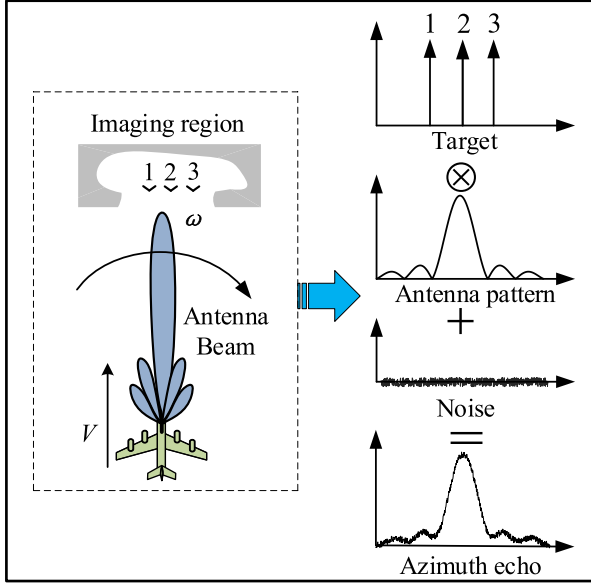


Fig. 1. Process of radar forward-looking imaging.

and

$$\mathbf{H} = \begin{bmatrix} h_1 & 0 & \cdots & 0 \\ h_2 & h_1 & \ddots & \vdots \\ \vdots & h_2 & \ddots & 0 \\ h_L & \vdots & \ddots & h_1 \\ 0 & h_L & \vdots & h_2 \\ \vdots & \ddots & \ddots & \vdots \\ 0 & \cdots & 0 & h_L \end{bmatrix} \quad (6)$$

The abovementioned modeling process of azimuth echo of radar forward-looking imaging can be directly shown in Fig. 1, where V is the platform speed and ω is the antenna scanning speed. It can be seen that the effect of noise makes the echo full of burrs, so the echo \tilde{s} received by the radar receiver will deviate from the true convolution result s .

Recovering real targets \mathbf{f} from the noise-polluted echo \tilde{s} is extremely ill-posed. Some typical methods, such as inverse filtering and least squares, can make the estimated target deviate greatly from the real value.

III. REVIEW OF TV-SPARSE METHOD

In this section, the TV-sparse method is reviewed to recover target distribution \mathbf{f} from the noise-polluted echo \tilde{s} , and the computational complexity is analyzed.

A. TV-Sparse Method

To simultaneously consider resolution improvement and contour preservation, the TV-sparse method requires solving following optimization problem,

$$\hat{\mathbf{f}} = \min_{\mathbf{f}} \frac{\mu}{2} \|\mathbf{A}\mathbf{f} - \tilde{s}\|_2^2 + \|\nabla \mathbf{f}\|_1 + \|\mathbf{f}\|_1 \quad (7)$$

where $\|\nabla \mathbf{f}\|_1$ denotes the TV term, which is used to preserve the contour information of the target, $\|\mathbf{f}\|_1$ is a sparse term to improve resolution, and

$$\nabla = \begin{bmatrix} -1 & 1 & & & \\ & -1 & 1 & & \\ & & \ddots & \ddots & \\ & & & -1 & 1 \\ & & & & -1 \end{bmatrix}$$

Thus, the superresolution problem of radar forward-looking imaging is transformed into a multiconstraint problem in the regularization framework. The solution to the multiconstraint problem is the image of the radar forward-looking region that we need. It can be seen that (7) consists of L_2 norm and L_1 norm. Since both L_2 norm and L_1 norm are convex functions, we use convex optimization method to solve (7). In previous work, it has been solved by three subproblems [25]

Subproblem 1: Solving the \mathbf{f} problem

$$\mathbf{f}^{k+1} = \mathbf{F}^{-1} \mathbf{g}^k \quad (8)$$

where

$$\mathbf{F} = (\mu \mathbf{A}^T \mathbf{A} + \gamma_1 \mathbf{\Delta} + \gamma_2 \mathbf{I})$$

$$\mathbf{g}^k = (\mu \mathbf{A}^T \tilde{s} + \gamma_1 \mathbf{D} (\mathbf{d}_1^k - \mathbf{b}_1^k) + \gamma_2 (\mathbf{d}_2^k - \mathbf{b}_2^k))$$

$$\mathbf{\Delta} = \begin{bmatrix} -1 & 1 & & & \\ 1 & -2 & \ddots & & \\ & 1 & \ddots & 1 & \\ & & \ddots & -2 & 1 \\ & & & 1 & -1 \end{bmatrix}$$

\mathbf{I} denotes identity matrix and $\mathbf{D} = -\nabla^*$.

Subproblem 2: Solving the \mathbf{d} problem

$$\begin{aligned} \mathbf{d}_1^{k+1} &= \text{shrink}(\nabla(\mathbf{f}^{k+1}) + \mathbf{b}_1^k, 1/\gamma_1) \\ \mathbf{d}_2^{k+1} &= \text{shrink}(\nabla(\mathbf{f}^{k+1}) + \mathbf{b}_2^k, 1/\gamma_2) \end{aligned} \quad (9)$$

where $\text{shrink}(x, \kappa) = \text{sign}(x) \max(|x| - \kappa, 0)$.

Subproblem 3: Solving the \mathbf{b} problem

$$\begin{aligned} \mathbf{b}_1^{k+1} &= \mathbf{b}_1^k + \nabla(\mathbf{f}^{k+1}) - \mathbf{d}_1^{k+1} \\ \mathbf{b}_2^{k+1} &= \mathbf{b}_2^k + \nabla(\mathbf{f}^{k+1}) - \mathbf{d}_2^{k+1} \end{aligned} \quad (10)$$

where \mathbf{d} and \mathbf{b} are two variables.

B. Analysis of Computational Complexity

The TV-sparse method requires iterating three subproblems to estimate the target distribution \mathbf{f} from the noise-polluted echo \tilde{s} , i.e., iterating (8)~(10). However, the main computational complexity comes from (8) because it includes matrix multiplication and inversion. As for solving (9) and (10), they only involve some simple addition and subtraction operations and, so, the computational complexity is very low. Compared with

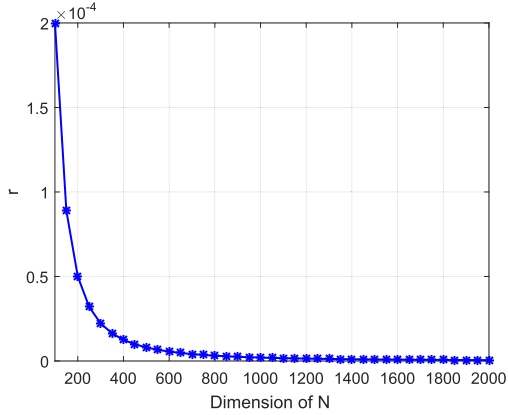


Fig. 2. Approximation error with dimension N .

$2N - 1$ of \mathbf{Q}_2 . Therefore, the multiplication of \mathbf{Q} and a vector can be obtained by intercepting the 1 to N elements of the FFT of \mathbf{q} and the vector. As for the multiplication of \mathbf{Q}^H and a vector, it can be obtained by the N to $2N - 1$ elements of the FFT of $\tilde{\mathbf{q}}$ and the vector, where $\tilde{\mathbf{q}} = [q_N^* \ q_{N-1}^* \ \cdots \ q_1^*]^T$. In the same way, $\mathbf{W}\mathbf{W}^H \mathbf{g}^k$ also can be obtained by two FFTs and truncations.

B. Analysis of Error

The proposed FTV-sparse method uses GS representation to realize fast computation. However, in order to realize the acceleration, we make some approximation, that is, Δ is approximated by $\tilde{\Delta}$. This approximation makes \mathbf{F} become $\tilde{\mathbf{F}}$, which affects the estimation of \mathbf{f} . Here, we define approximation error to measure the effect of this approximation. The approximation error is defined as

$$r = \frac{1}{N \times N} \left\| \mathbf{F} - \tilde{\mathbf{F}} \right\|_2 \quad (22)$$

where r is the approximation error.

The approximation error curve with dimension N is shown in Fig. 2. This shows that the error caused by the approximation is quite small. Even when $N = 100$, the error is only 2×10^{-4} , and the error decreases with the increase of the dimension. In radar imaging, the dimension of echo is usually large, so the above-mentioned approximation has little effect on the superresolution performance and can be ignored.

C. Analysis of Computational Complexity

The computational complexity analysis of the proposed method is as follows. First, we also need to calculate $\mathbf{A}^T \tilde{\mathbf{s}}$ once, and the computational complexity is $O(N \log N)$. Second, For each iteration, using the Levinson–Durbin algorithm to calculate the autoregressive coefficients \mathbf{c} and prediction error e , the computational complexity is $O((N - 1)^2)$. Then, the solution of (19) can be achieved by four Toeplitz vector operations, for which the computational complexity is $O(14N \log(2N) + N(2N - 1) + 7N)$ [31]. Hence, the computational complexity of the proposed method

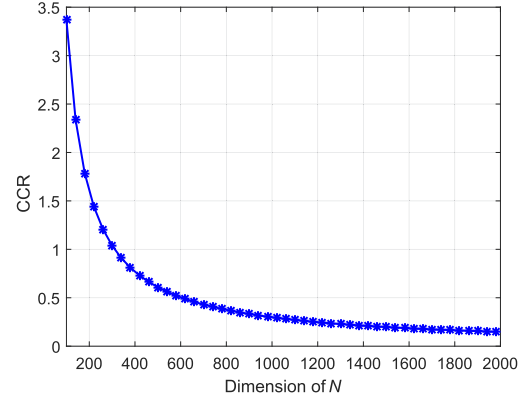


Fig. 3. CCR of the proposed method and TV-sparse method.

is $O(K((N - 1)^2 + 14N \log(2N) + N(2N - 1) + 7N) + O(N \log N))$.

Therefore, after acceleration, the computational complexity of the algorithm is reduced from the third order to the second order of N . For visually finding the difference of computational complexity before and after acceleration, we empirically assume that $K = 30$ and plot the computational cost ratio (CCR) of the proposed method and TV-sparse method, as shown in Fig. 3. The CCR is defined as

$$\text{CCR} = \frac{C_{\text{FTV-s}}}{C_{\text{TV-s}}} \times 100\% \quad (23)$$

where $C_{\text{FTV-s}}$ is the computational complexity of the proposed FTV-sparse method and $C_{\text{TV-s}}$ is the computational complexity of the TV-sparse method.

From Fig. 3, we can find that the calculation cost of the proposed method is much less than that of the TV-sparse method, and the computational advantage of the proposed method increases with the increase of dimension N , which greatly reduces the computational complexity and improves the real-time imaging ability, in practice.

D. Selection of Parameters

For the proposed method, we can see that there are three parameters which need to be identified, i.e., μ , γ_1 , and γ_2 . In our work, the parameters are selected by the L -curve method [37], [38].

For the parameter μ , we defined that $\mathbf{p}_1^k = \mathbf{d}_1^k - \mathbf{b}_1^k$, $\mathbf{p}_2^k = \mathbf{d}_2^k - \mathbf{b}_2^k$, $\mathbf{r}_1 = \nabla \mathbf{f} - \mathbf{p}_1^k$ and $\mathbf{r}_2 = \nabla \mathbf{f} - \mathbf{p}_2^k$. The L -curve consists of plotting $\log(\frac{\gamma_1}{2} \|\mathbf{r}_1\|_2^2 + \frac{\gamma_2}{2} \|\mathbf{r}_2\|_2^2)$ as a function of $\log(\frac{1}{2} \|\mathbf{A}\mathbf{f} - \tilde{\mathbf{s}}\|_2^2)$. Then, the parameter μ is found at the corner of the L -curve.

Using the L -curve method, the optimal γ_1 and γ_2 are found as the corners of the L -curve constructed by plotting $\log(\|\mathbf{d}_1\|_1)$ as a function of $\log(\frac{1}{2} \|\mathbf{d}_1 - \nabla(\mathbf{f}^{k+1}) - \mathbf{b}_1^k\|_2^2)$ and $\log(\|\mathbf{d}_2\|_1)$ as a function of $\log(\frac{1}{2} \|\mathbf{d}_2 - \nabla(\mathbf{f}^{k+1}) - \mathbf{b}_2^k\|_2^2)$, respectively.

In particular, at the first iteration, the parameters γ_1 and γ_2 are first selected by experience, then the parameter μ can be

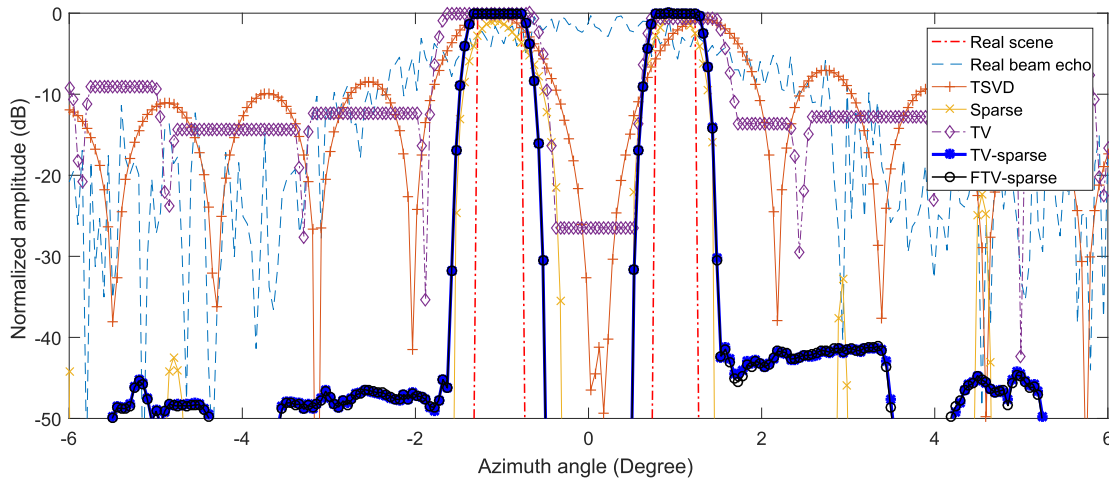


Fig. 4. Simulation results with the SNR of 20 dB.

determined by L -curve. In the rest of the iteration, γ_1 and γ_2 are automatically updated according to L -curve.

V. VERIFICATION OF PERFORMANCE

In this section, experiments are conducted to verify the performance of the proposed method. We first design a simulation of two adjacent targets, to demonstrate the performance resolution improvement and contour preservation of the proposed method. Then, two measured data are processed to verify the performance of the proposed method in practice. Finally, we build a hardware platform based on field programmable gate array (FPGA), and test the computing time of the proposed FTV-sparse method and the traditional TV-sparse method in practice. Meanwhile, the result is compared with TSVD, sparse, TV and TV-sparse methods.

A. Simulation

A simulation of point targets is first utilized to demonstrate the performance of the proposed method. For the simulation, a sinc² function is employed as the antenna pattern, and its beam width is 3°. The real scene includes two adjacent point targets whose center is at -1° and 1° , respectively. The width of each target is 0.6° . The scanning region is $\pm 6^\circ$. It can be seen that the minimum interval of adjacent targets is 1.4° . According to Rayleigh criterion, they will not be distinguished by real aperture imaging.

The simulation is carried out under the condition that the SNR is 20 dB, where SNR is defined as

$$\text{SNR} = 20 \log_{10} \frac{\|\mathbf{f}\|_2^2}{\|\mathbf{A}\mathbf{f} - \tilde{\mathbf{s}}\|_2^2} \quad (24)$$

The simulation results are shown in Fig. 4. We can see that the adjacent targets cannot be distinguished in real-beam echo. TSVD can distinguish the targets to a certain degree, but the sidelobes are raised, and the contour of targets is missing. Sparse method can distinguish adjacent targets and suppress noise, but it cannot preserve the contour of the target. TV method can

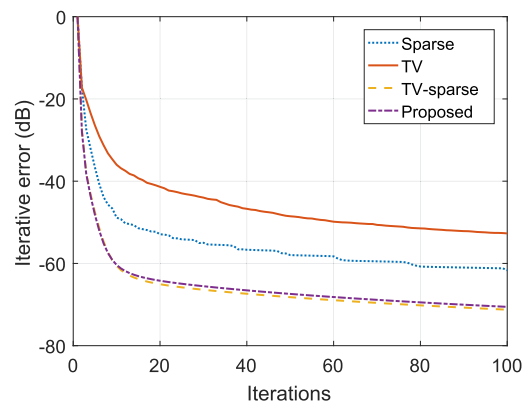


Fig. 5. Iterative error with SNR of 20 dB.

preserve the contour of the target, but the resolution is low and the noise amplification is serious. TV-sparse and proposed methods can distinguish the adjacent targets and preserve the target contour, and have better noise suppression ability than TV method. In addition, the results of TV-sparse and proposed are almost overlapped, which shows that the performance of the algorithm will not be degenerated after acceleration.

The iterative error curves of different algorithm are plotted in Fig. 5, where the iterative error is defined as

$$\text{error} = 10 \log_{10} \left\| \tilde{\mathbf{f}}^{k+1} - \tilde{\mathbf{f}}^k \right\|_2^2 \quad (25)$$

These curves shows that with the increase of the iterations, the iterative errors of TV-sparse method and proposed method are much smaller than those of TV and sparse method, and the iterative errors of TV-sparse method and proposed method are almost the same, which shows that TV sparse method and proposed method have better convergence ability. So their results are closer to the original scene.

For further verification, we calculate the mean square error (MSE) of the results of different methods. The MSE is defined

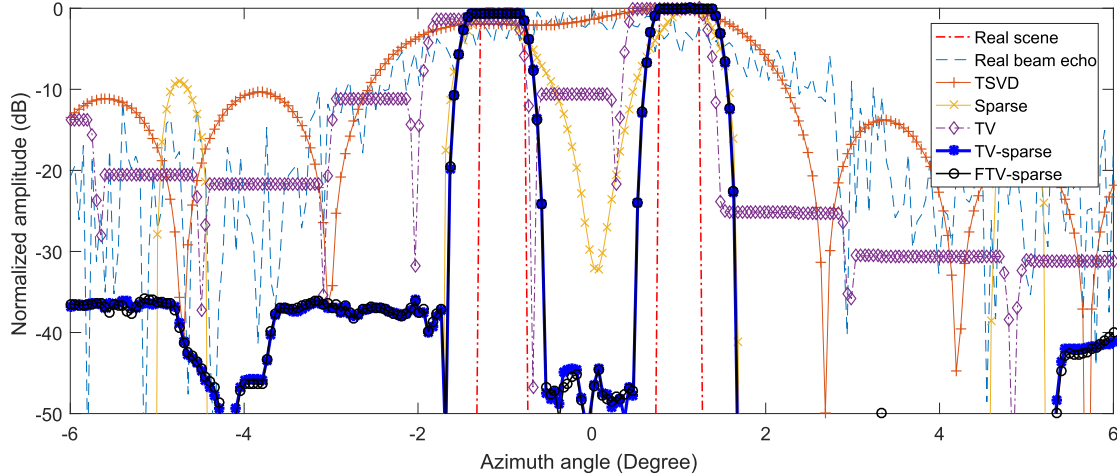


Fig. 6. Simulation results with the SNR of 10 dB.

TABLE I
MSES WITH SNR OF 20 dB

Methods	TSVD	Sparse	TV	TV-sparse	Proposed
MSE	0.0204	0.0092	0.0231	0.0084	0.0084

as

$$\text{MSE} = \frac{1}{N_c} \sum_{i=1}^{N_c} \frac{1}{N} \left\| \widehat{\mathbf{f}}_i - \mathbf{f} \right\|_2^2 \quad (26)$$

where N_c is the number of Monte-Carlo experiments. The smaller the MSE indicates that the superresolution result is closer to the real scene. In this simulation, we let $N_c = 100$, then the MSEs are shown in Table I. MSEs also shows that the superresolution results of TV-sparse and proposed methods are almost the same, and they are closer to the real scene.

In radar imaging, sometimes it suffers from strong noise. Therefore, the performance of the proposed method is demonstrated at the condition of low SNR. We repeat abovementioned simulation and let $\text{SNR} = 10$ dB, and the simulation results are illustrated in Fig. 6. It can be seen that with the decrease of SNR, the performance of all algorithms has degenerated. TSVD method is unable to distinguish adjacent targets completely. Sparse and TV method can distinguish adjacent targets, but affected by strong noise, false targets appear. The TV-sparse and the proposed methods cannot only distinguish adjacent targets, but also preserve the contour of the targets. Although the noise is amplified partly, the noise amplitude is almost below -15 dB, which hardly affected target recognition in practice. The iterative error curves are shown in Fig. 7. At low SNR condition, the TV-sparse and the proposed methods still have good convergence performance, and the iterative error after convergence is much smaller than other methods. In addition, the superresolution results and iteration error curves of the TV-sparse and proposed methods almost overlap, which shows

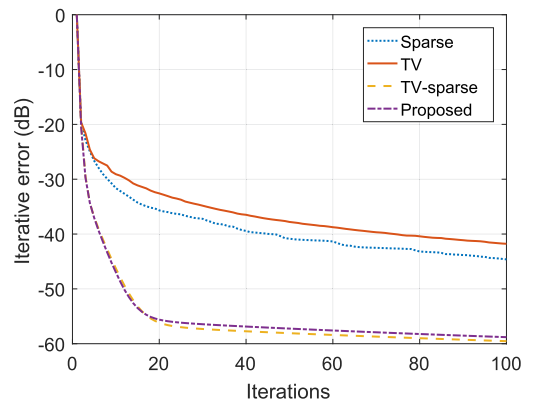


Fig. 7. Iterative error with SNR of 10 dB.

TABLE II
MSE WITH SNR OF 10 dB

Methods	TSVD	Sparse	TV	TV-sparse	Proposed
MSE	0.0281	0.0128	0.0185	0.0117	0.0118

that the acceleration strategy used in this article will hardly cause performance degradation.

The MSEs of different superresolution are also shown in Table II, and the results are consistent with the abovementioned conclusion.

B. Measured Data Verification

The simulation has demonstrated the effectiveness of the proposed method. However, it should be pointed out that the abovementioned simulation is performed under the condition of ideal noise, that is, Gaussian white noise. Conditions in practice are usually more complex than ideal. Therefore, the measured data are processed to verify the performance of the proposed method in practice.

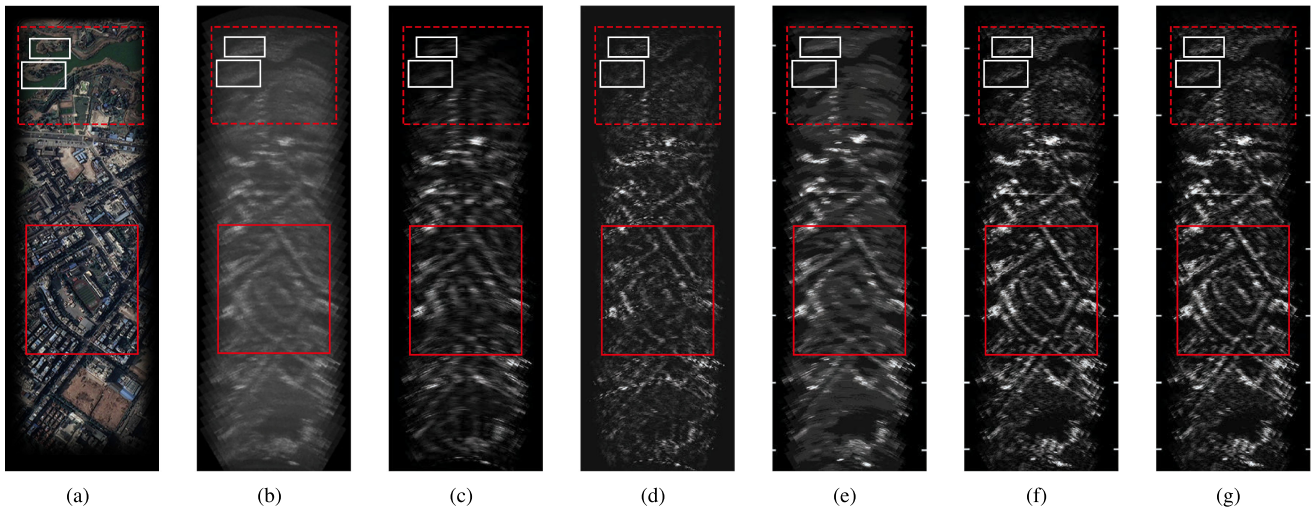


Fig. 8. Superresolution results of measured data. (a) Optical scenario. (b) Real-beam echo. (c) TSVD. (d) Sparse. (e) TV. (f) TV-sparse. (g) Proposed.

TABLE III
SYSTEM PARAMETERS OF MEASURED DATA

Parameter	Value	Units
Beamwidth	4	$^{\circ}$
Carrier frequency	30.75	GHz
Band width	200	MHz
Antenna scanning velocity	60	$^{\circ}/s$
Antenna scanning area	- 30 ~ 30	$^{\circ}$
Pulse repetition frequency	500	Hz

1) *Ground Data*: A ground data are first processed. The data were collected at the Luodai town, Chengdu, China. The system parameters are shown in Table III. The optical scene intercepted from Google Earth is shown in Fig. 8(a). We can see that the red dotted rectangle on the upper part of the optical scene marks a lake. There are two obvious islands in the lake, which are marked with white solid rectangle. In addition, the red solid line rectangle in the lower part of the optical scene marks a school, and the roads around the school are clear.

The real-beam echo is shown in Fig. 8(b). It can be seen that the resolution of real-beam echo is low and the picture is fuzzy. Fig. 8(c) to (g) shows the superresolution results processed by TSVD, sparse, TV, TV-sparse and proposed methods. In this experiment, TSVD, sparse, and TV methods only achieve limited improvement in resolution, resulting in unclear contours of lake and roads. However, TV-sparse and the proposed method still have good superresolution ability. In their superresolution results, the contour of lake and road is clear. Besides, the entropy is utilized to quantitatively evaluate the performance of different methods. According to minimum entropy principle, the smaller the image entropy, the clearer the image [39]. As shown in Table IV, the entropies of superresolution results of TV-sparse and proposed methods is the same and less than that of other methods, which also shows that TV-sparse and the proposed TV-sparse method has better superresolution effect than other

TABLE IV
ENTROPIES OF GROUND DATA PROCESSING

Methods	Real-beam	TSVD	Sparse	TV	TV-sparse	Proposed
Entropy	2.77	2.26	2.06	2.58	1.67	1.67

TABLE V
SYSTEM PARAMETERS OF MEASURED DATA

Parameter	Value	Units
Beamwidth	3	$^{\circ}$
Carrier frequency	9.6	GHz
Band width	200	MHz
Antenna scanning velocity	18	$^{\circ}/s$
Pulse repetition frequency	800	Hz

methods. Therefore, their superresolution results are clearer than that of other methods.

Fig. 9 and Fig. 10 show the partially enlarged pictures of the lake and school. The results further prove that the superresolution result of TV-sparse and the proposed TV-sparse method better preserves the contour of the scene, so the lake and the roads around school are more clear and distinguishable than those of other methods.

By comparing the results of TV-sparse and the proposed methods, it can be found that their superresolution results are almost identical. This confirms again that the acceleration strategy used in this article will hardly cause performance degradation in practice.

2) *Sea Surface Data*: Another measured data were collected on a sea surface. The system parameters of radar are listed in Table V.

The imaging area of this experiment contains land and ocean. The processed results are shown in Fig. 11, where Fig. 11(a) is the real beam echo with low resolution. It can be seen that

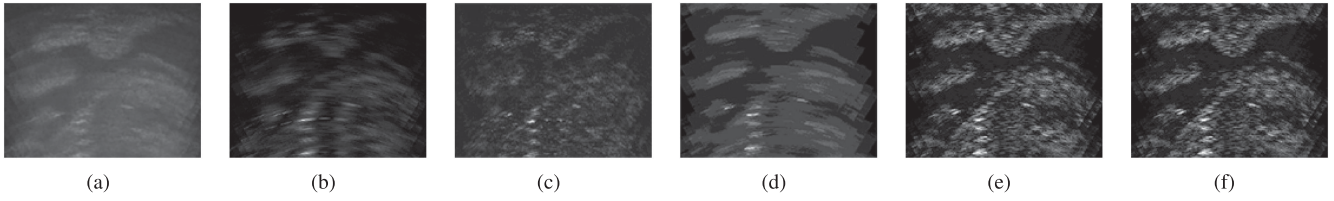


Fig. 9. Partial enlarged drawings for lake in Fig. 8. (a) Real-beam echo. (b) TSVD. (c) Sparse. (d) TV. (e) TV-sparse. (f) Proposed.

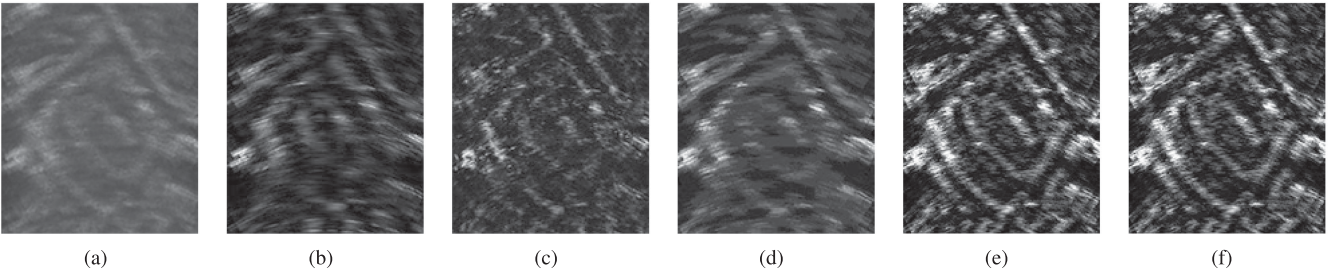


Fig. 10. Partial enlarged drawings for school in Fig. 8. (a) Real-beam echo. (b) TSVD. (c) Sparse. (d) TV. (e) TV-sparse. (f) Proposed.

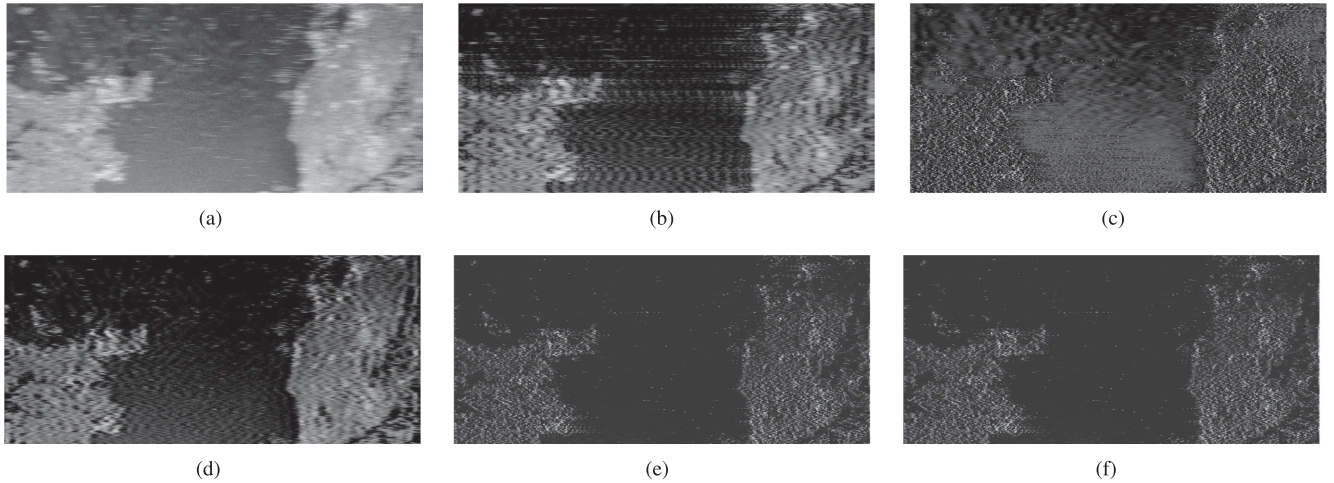


Fig. 11. Superresolution results of sea surface data. (a) Real-beam echo. (b) TSVD. (c) Sparse. (d) TV. (e) TV-sparse. (f) Proposed.

the contour of the land is blurred and accompanied by strong noise. Fig. 11(b) to (d) is the superresolution results of TSVD, sparse, and TV methods. These results show that although TSVD, sparse, and TV methods improve the resolution, the improvement in resolution is limited and the contour of the land is not clear. In particular, because of the low SNR of the measured data, the TV method does not recover the land contour very well. Fig. 11(e) and (f) shows the superresolution results of TV-sparse and FTV-sparse methods. It can be seen that these two methods can effectively improve the resolution and suppress noise. Their superresolution results show clear land contours and distinct land-sea divisions.

The entropies of different results are shown in Table VI. It also shows that the superresolution results of TV-sparse and FTV-sparse methods are clearer than that of other methods, and

TABLE VI
ENTROPIES OF SEA SURFACE DATA PROCESSING

Methods	Real-beam	TSVD	Sparse	TV	TV-sparse	Proposed
Entropy	8.21	6.99	3.59	4.04	2.85	2.86

the TV-sparse and FTV-sparse methods have almost the same performance.

C. Assessment of Computing Time

In Section IV-C, the CCR curves have shown the computational advantage of the proposed method. In practice, the data are usually processed by a FPGA or digital signal processing

TABLE VII
COMPUTING TIME OF DIFFERENT ALGORITHMS

Methods	CTs of ground data	CTs of sea surface data
TSVD	72.94	2789.35
Sparse	147.81	3585.64
TV	157.67	3765.24
TV-sparse	159.31	3826.92
FTV-sparse	1.26	12.28

chip. Here, we used an eight-core TMS320c6678 chip produced by Texas Instruments (TI) as an example to build a hardware platform, and tested the computing time of different algorithms. The main frequency is 1GHz and the memory is 4GB.

For abovementioned measured data, their echo dimensions are 1600×500 and 1301×2855 , where $a \times b$ represents a samples in range and b samples in azimuth. Based on the hardware platform, the computing times (CTs) of the different algorithms are listed in Table VII. The results show that the computing time of proposed method is greatly reduced after acceleration. The computational efficiency is increased by about 191 times for the ground data and 312 times for the sea surface data.

VI. CONCLUSION

In this article, we proposed a FTV-sparse method to reduce the computational complexity of traditional TV-sparse method in radar forward-looking imaging. According to the Toeplitz property of the measurement matrix in traditional TV-sparse method, we use GS representation to solve the linear equations quickly, skillfully avoiding the matrix inversion operation.

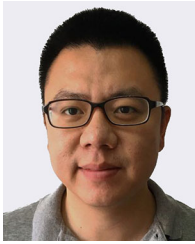
Through both simulation and measured data processing experiments, we demonstrated that the proposed method almost does not cause performance degradation compared with the traditional TV-sparse method. The hardware test shows that for the echo with dimension of 1600×500 and 1301×2855 , the computational efficiency of the proposed method is about 191 and 312 times that of the traditional TV-sparse method, respectively.

REFERENCES

- [1] M. Ressler, L. Nguyen, F. Koenig, D. Wong, and G. Smith, "The army research laboratory (ARL) synchronous impulse reconstruction (SIRE) forward-looking radar," *Proc. SPIE*, vol. 6561, 2007, Art. no. 656105.
- [2] F. Soldovieri, G. Gennarelli, I. Catapano, D. Liao, and T. Dogaru, "Forward-looking radar imaging: A comparison of two data processing strategies," *IEEE J. Sel. Top. Appl. Earth Observ. Remote Sens.*, vol. 10, no. 2, pp. 562–571, Feb. 2017.
- [3] J. G. Verly and R. L. Delanoy, "Model-based automatic target recognition (ATR) system for forwardlooking groundbased and airborne imaging laser radars (LADAR)," *Proc. IEEE*, vol. 84, no. 2, pp. 126–163, Feb. 1996.
- [4] W. Li, W. Zhang, Q. Zhang, Y. Zhang, Y. Huang, and J. Yang, "Simultaneous super-resolution and target detection of forward-looking scanning radar via low-rank and sparsity constrained method," *IEEE Trans. Geosci. Remote Sens.*, vol. 58, no. 10, pp. 7085–7095, Oct. 2020.
- [5] F. Biondi, "Recovery of partially corrupted SAR images by super-resolution based on spectrum extrapolation," *IEEE Geosci. Remote Sens. Lett.*, vol. 14, no. 2, pp. 139–143, Feb. 2017.
- [6] Y. Zhang, Q. Zhang, Y. Zhang, J. Pei, and J. Yang, "Fast split bregman based deconvolution algorithm for airborne radar imaging," *Remote Sens.*, vol. 12, no. 11, 2020, Art. no. 1747.

- [7] F. Biondi, "SAR tomography optimization by interior point methods via atomic decomposition—The convex optimization approach," in *Proc. IEEE Geosci. Remote Sens. Symp.*, 2014, pp. 1879–1882.
- [8] R. Heckel, V. I. Morgenshtern, and M. Soltanolkotabi, "Super-resolution radar," *Inf. Inference, J. IMA*, vol. 5, no. 1, pp. 22–75, 2016.
- [9] W. U. Bajwa, K. Gedalyahu, and Y. C. Eldar, "Identification of parametric underspread linear systems and super-resolution radar," *IEEE Trans. Signal Process.*, vol. 59, no. 6, pp. 2548–2561, Jun. 2011.
- [10] N. Nguyen, P. Milanfar, and G. Golub, "A computationally efficient super-resolution image reconstruction algorithm," *IEEE Trans. Image Process.*, vol. 10, no. 4, pp. 573–583, Apr. 2001.
- [11] Y. Zhang, A. Jakobsson, Y. Zhang, Y. Huang, and J. Yang, "Wideband sparse reconstruction for scanning radar," *IEEE Trans. Geosci. Remote Sens.*, vol. 56, no. 10, pp. 6055–6068, Oct. 2018.
- [12] F. Sadjadi, "Radar beam sharpening using an optimum FIR filter," *Circuits Syst. Signal Process.*, vol. 19, no. 2, pp. 121–129, 2000.
- [13] J. D. Shea, B. D. Van Veen, and S. C. Hagness, "A TSVD analysis of microwave inverse scattering for breast imaging," *IEEE Trans. Biomed. Eng.*, vol. 59, no. 4, pp. 936–945, Apr. 2012.
- [14] S. Kidera, T. Sakamoto, and T. Sato, "Super-resolution UWB radar imaging algorithm based on extended capon with reference signal optimization," *IEEE Trans. Antennas Propag.*, vol. 59, no. 5, pp. 1606–1615, May 2011.
- [15] P. Stoica, Z. Wang, and L. Jian, "Robust Capon beamforming," *IEEE Signal Process. Lett.*, vol. 10, no. 6, pp. 172–175, Jun. 2003.
- [16] K.-T. Kim, D.-K. Seo, and H.-T. Kim, "Efficient radar target recognition using the MUSIC algorithm and invariant features," *IEEE Trans. Antennas Propag.*, vol. 50, no. 3, pp. 325–337, Mar. 2002.
- [17] T. Kailath and A. Lee Swindlehurst, "A performance analysis of subspace-based methods in the presence of model errors: Part I—the music algorithm," *IEEE Trans. Signal Process.*, vol. 40, no. 7, pp. 1758–1774, Jul. 1992.
- [18] Y. Zhang, D. Mao, Q. Zhang, Y. Zhang, Y. Huang, and J. Yang, "Airborne forward-looking radar super-resolution imaging using iterative adaptive approach," *IEEE J. Sel. Top. Appl. Earth Observ. Remote Sens.*, vol. 12, no. 7, pp. 2044–2054, Jul. 2019.
- [19] T. Yardibi, J. Li, P. Stoica, M. Xue, and A. B. Baggeroer, "Source localization and sensing: A nonparametric iterative adaptive approach based on weighted least squares," *IEEE Trans. Aerosp. Electron. Syst.*, vol. 46, no. 1, pp. 425–443, Jan. 2010.
- [20] Q. Zhang, Y. Zhang, Y. Huang, and Y. Zhang, "Azimuth superresolution of forward-looking radar imaging which relies on linearized bregman," *IEEE J. Sel. Top. Appl. Earth Observ. Remote Sens.*, vol. 12, no. 7, pp. 2032–2043, Jul. 2019.
- [21] W. Li, M. Niu, Y. Zhang, Y. Huang, and J. Yang, "Forward-looking scanning radar superresolution imaging based on second-order accelerated iterative shrinkage-thresholding algorithm," *IEEE J. Sel. Top. Appl. Earth Observ. Remote Sens.*, vol. 13, pp. 620–631, 2020.
- [22] C. Poon and G. Peyré, "Multidimensional sparse super-resolution," *SIAM J. Math. Anal.*, vol. 51, no. 1, pp. 1–44, 2019.
- [23] J. Ma, C. Chen, C. Li, and J. Huang, "Infrared and visible image fusion via gradient transfer and total variation minimization," *Inf. Fusion*, vol. 31, pp. 100–109, 2016.
- [24] L. Condat, "Discrete total variation: New definition and minimization," *SIAM J. Imag. Sci.*, vol. 10, no. 3, pp. 1258–1290, 2017.
- [25] Q. Zhanget al., "TV-sparse super-resolution method for radar forward-looking imaging," *IEEE Trans. Geosci. Remote Sens.*, vol. 58, no. 9, pp. 6534–6549, Sep. 2020.
- [26] Y. Zhang, Y. Zhang, W. Li, Y. Huang, and J. Yang, "Super-resolution surface mapping for scanning radar: Inverse filtering based on the fast iterative adaptive approach," *IEEE Trans. Geosci. Remote Sens.*, vol. 56, no. 1, pp. 127–144, Jan. 2018.
- [27] K. H. Jin, D. Lee, and J. C. Ye, "A general framework for compressed sensing and parallel MRI using annihilating filter based low-rank Hankel matrix," *IEEE Trans. Computat. Imag.*, vol. 2, no. 4, pp. 480–495, Dec. 2016.
- [28] T. Kailath, "Some new algorithms for recursive estimation in constant linear systems," *IEEE Trans. Inf. Theory*, vol. 19, no. 6, pp. 750–760, Nov. 1973.
- [29] G.-O. Glentis and A. Jakobsson, "Efficient implementation of iterative adaptive approach spectral estimation techniques," *IEEE Trans. Signal Process.*, vol. 59, no. 9, pp. 4154–4167, Sep. 2011.
- [30] Y. Zhang, Q. Zhang, Y. Zhang, J. Pei, Y. Huang, and J. Yang, "Fast split Bregman based deconvolution algorithm for airborne radar imaging," *Remote Sens.*, vol. 12, no. 11, 2020, Art. no. 1747.

- [31] J. Karlsson, W. Rowe, L. Xu, G. O. Glentis, and J. Li, "Fast missing-data IAA with application to notched spectrum SAR," *IEEE Trans. Aerosp. Electron. Syst.*, vol. 50, no. 2, pp. 959–971, Apr. 2014.
- [32] M. Cetin and W. C. Karl, "Feature-enhanced synthetic aperture radar image formation based on nonquadratic regularization," *IEEE Trans. Image Process.*, vol. 10, no. 4, pp. 623–631, Apr. 2001.
- [33] X. X. Zhu and R. Bamler, "Tomographic SAR inversion by L_1 -norm regularization—The compressive sensing approach," *IEEE Trans. Geosci. Remote Sens.*, vol. 48, no. 10, pp. 3839–3846, Oct. 2010.
- [34] P. Stoica *et al.*, *Spectral Analysis of Signals* Englewood Cliffs, NJ, USA: Prentice-Hall, 2005.
- [35] G.-O. Glentis and A. Jakobsson, "Superfast approximative implementation of the iaa spectral estimate," *IEEE Trans. Signal Process.*, vol. 60, no. 1, pp. 472–478, Jan. 2012.
- [36] J. R. Jensen, G.-O. Glentis, M. G. Christensen, A. Jakobsson, and S. H. Jensen, "Fast LCMV-based methods for fundamental frequency estimation," *IEEE Trans. Signal Process.*, vol. 61, no. 12, pp. 3159–3172, Jun. 2013.
- [37] P. C. Hansen and D. P. O'Leary, "The use of the L-curve in the regularization of discrete ill-posed problems," *SIAM J. Sci. Comput.*, vol. 14, no. 6, pp. 1487–1503, 1993.
- [38] D. Calvetti, L. Reichel, and A. Shuibi, "L-curve and curvature bounds for Tikhonov regularization," *Numer. Algorithms*, vol. 35, no. 2/4, pp. 301–314, 2004.
- [39] K. Ghasedi Dizaji, A. Herandi, C. Deng, W. Cai, and H. Huang, "Deep clustering via joint convolutional autoencoder embedding and relative entropy minimization," in *Proc. IEEE Int. Conf. Comput. Vis.*, 2017, pp. 5736–5745.



Yin Zhang (Member, IEEE) received the B.S. and Ph.D. degrees in electronic information engineering from the University of Electronic Science and Technology of China (UESTC), Chengdu, China, in 2008 and 2016, respectively.

From 2015 to 2016, he was a Visiting Student with the University of Delaware, Newark, DE, USA. He is currently an Associate Research Fellow with the School of Information and Communication Engineering, UESTC. His research interests include radar imaging and signal processing in related radar

applications.



Qiping Zhang (Graduate Student Member, IEEE) received the B.S. degree in electronic information engineering from the Yunnan University, Kunming, China, in 2016. He is currently working toward the Ph.D. degree in signal and information processing with the University of Electronic Science and Technology of China, Chengdu, China.

His research interests include signal processing and radar imaging.



Yongchao Zhang (Member, IEEE) received the B.S. degree in electronic information engineering from Hainan University, Haikou, China, in 2011. He received the Ph.D. degree in signal and information processing from the School of Information and Communication Engineering, University of Electronic Science and Technology of China (UESTC), Chengdu, China, in 2018.

From 2016 to 2017, he was a Visiting Student with Lund University, Lund, Sweden. He is currently an Associate Research Fellow with the School of Information and Communication Engineering, UESTC. His research interests include array signal processing and inverse problem in radar applications.



Yulin Huang (Senior Member, IEEE) received the B.S. degree in electronic and information engineering and Ph.D. degree in information acquisition and detection technology from the School of Electronic Engineering, University of Electronic Science and Technology of China (UESTC), Chengdu, China, in 2002 and 2008, respectively.

From 2013 to 2014, he was a Visiting Researcher with the University of Houston, Houston, TX, USA. He is currently a Professor with the School of Information and Communication Engineering, UESTC.

His research interests include SAR, target detection and recognition, artificial intelligence, and machine learning.



Jianyu Yang (Member, IEEE) received the B.S. degree in electronic and information engineering from the National University of Defense Technology, Changsha, China, in 1984, and the M.S. and Ph.D. degrees in communication and information system from the University of Electronic Science and Technology of China (UESTC), Chengdu, China, in 1987 and 1991, respectively.

He is currently a Professor with UESTC. His research interests include SAR and statistical signal processing. He is serving as a Senior Editor for the

Chinese Journal of Radio Science and the *Journal of Systems Engineering and Electronics*.